REVISTA MATÉRIA V.28 N.3
ISSN 1517-7076 articles e20230154, 2023

Research on an acoustic judgment method for the incipient cavitation of model hydraulic machinery runner blades

Wentao Su[1,2], Weijun Meng[1], Yue Zhao[2], Jian Wu[3], Yuekun Sun[4]

[1]Liaoning Petrochemical University, College of Petroleum Engineering. Fushun 113001, China.
[2]Harbin Institute of Large Electric Machinery, Harbin Electric Machinery Company Limited. Harbin 150040, China.
[3]Harbin Institute of Technology, School of Energy Science and Engineering. Harbin 150001, China.
[4]CHN Energy GHEI integrated smart energy Company Limited. Beijing 100007, China.
e-mail: suwentao@lnpu.edu.cn, 710437382@qq.com, zhaoyue@hec-china.com, jian.wu@hit.edu.cn, syk0409@126.com

ABSTRACT

The cavitation phenomenon is an important factor affecting the safe and stable operation of hydraulic machinery units. The cavitation of the hydraulic machinery units can lead to the increased vibration, reduced efficiency, and cavitation erosion of blades. Therefore, a method is needed to determine the incipient cavitation of hydraulic machinery runner blades. This study is initiated from the acoustic characteristics of bubbles generated by the cavitation of model hydraulic turbines and the characteristics of radiated sound energy during cavitation. The characteristics of cavitation noise are studied. After the qualitative analysis of the high- and low-frequency energy distribution patterns of cavitation noise signals before and after cavitation, a mathematical model of the time-frequency characteristics of these signals is proposed using the energy distribution analysis method. The feature information is extracted from the cavitation noise signals and used to judge the occurrence of incipient cavitation in model turbine runner blades. Based on this method, an online cavitation monitoring system is constructed, and comparative tests are carried out on a model pump turbine and Francis turbine. It is found that the results of the proposed method for the judgment of incipient cavitation are highly consistent with those of traditional methods.

Keywords: Cavitation; acoustic; hydraulic Machinery; model test.

1. INTRODUCTION

Hydraulic machinery is one of the most typical and widely used mechanical equipment [1]. It is not only the key equipment in water conservancy and hydropower, agricultural engineering, industrial production, and the energy and chemical industries, but also plays a vital role in military and aerospace applications, medicine and health, the nuclear power industry, and other fields. Cavitation is a common concern in the field of hydraulic machinery as shown in Figure 1. It not only leads to reduced hydraulic performance and excessive vibration and noise, but also causes cavitation damage to the flow components, thus posing a huge threat to safe and stable operation. Determining how to control and even prevent cavitation hazards has always been an important issue in the operation and maintenance of hydraulic machinery.

The industrial and academic communities have paid attention to the monitoring and diagnosis of cavitation phenomena in hydraulic machinery. Determining how to accurately judge whether hydraulic machinery has experienced cavitation and the specific development stage of cavitation have always been research hotspots and difficulties in related fields. The cavitation identification technology for hydraulic machinery is mainly divided into three categories, the first of which is cavitation judgment based on hydraulic performance [2]. This method is most commonly used in engineering, but its disadvantage is that it can only judge the fully developed cavitation state and cannot meet the requirements of cavitation prevention and control. The second type is cavitation recognition based on specific equipment [3], including high-speed photography technology, X-ray detection, ultrasonic detection, etc. These methods can directly observe or indirectly detect cavitation flow fields, resulting in high reliability. However, due to limitations in testing equipment and on-site conditions, they are difficult to promote in industrial sites. The third type is sensor-based cavitation characterization [4], such as pressure pulsation testing, acoustic emission acquisition, acoustic vibration measurement, etc. These methods are characterized by relatively simple installation and measurement, and have both engineering applicability

Corresponding Author: Weijun Meng Received on 16/05/2023 Accepted on 27/06/2023

DOI: https://doi.org/10.1590/1517-7076-RMAT-2023-0154

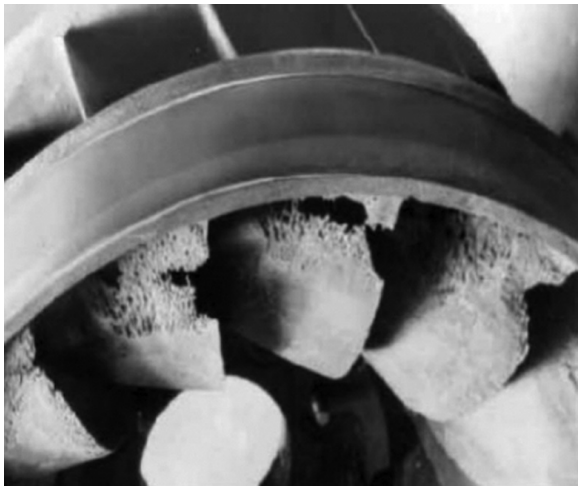

Figure 1: The blade cavitation phenomenon.

and diagnostic accuracy. In particular, acoustic vibration measurement is characterized by convenient installation, simple testing, and rich information, making it an ideal way to identify cavitation. However, due to the complexity and variability of cavitation phenomena, as well as the strong interference of acoustic and vibration signals, the study of cavitation state characterization in hydraulic machinery requires high requirements for signal processing and feature extraction. The further development of specialized methods based on classical signal processing methods is needed.

The formation, development, oscillation, falling off, and collapse of cavitation will induce acoustic vibration, so many scholars have used acoustic vibration signals to characterize and study the cavitation status of hydraulic machinery. BAJIC [5] mainly used a vibration and noise monitoring method to carry out the cavitation monitoring and identification of hydraulic turbines. Via this method, the cavitation degree of hydraulic turbines is comprehensively evaluated by collecting the noise in the draft tube and combining the efficiency of hydraulic turbines. Due to the difficulty and low sensitivity of cavitation noise extraction, this method has not been widely promoted [6]. ESCALER *et al.* [7] proposed a digital envelope detection method for vibration signals based on the theory of vibration envelope spectrum detection. He studied the vibration signals at the guide bearings and guide vanes of a model hydraulic turbine that had undergone cavitation. It was found that the envelope spectrum had peaks at the rotational frequency, blade channel frequency, guide vane characteristic frequency, and some multiples of the frequency. Based on this, it was believed that these peaks were characteristics of hydraulic turbine cavitation and could be used for cavitation detection. However, the experimental results had no theoretical basis for linking cavitation phenomena (high-frequency) with certain characteristic frequencies (low-frequency) of hydraulic turbines. PENDAR and PASCOA [8] and KOLAHAN *et al.* [9] used Fourier transform and wavelet analysis to identify and characterize various cavitation states, including cloud cavitation. ČUDINA [10] collected the aerodynamic noise of centrifugal pumps and peeled off characteristic spectral lines from the noise spectrum to monitor the inception and development of cavitation. HU *et al.* [11] monitored the underwater acoustic signal at the inlet of the pump, and found that the underwater sound first increased and then decreased during cavitation development. Its low-frequency characteristics can be used to determine the occurrence of cavitation. LIU *et al.* [12] conducted time- and frequency-domain analyses of propeller cavitation via underwater sound, and found that cavitation sound has a strong impact. As cavitation develops, the number and amplitude of sound pulses gradually increase. RAMADEVI [13] and HE and LIU [14] utilized discrete wavelet transform to detect the inception and different forms of cavitation. These researchers all attempted to search for a specific characteristic frequency or frequency band that occurs when cavitation occurs. However, during the operation of hydraulic machinery, regardless of whether or what type of cavitation occurs, the sound signal radiated by cavitation covers the frequency range that can be analyzed by the entire collection system. Therefore, the analysis of the energy signal of cavitation radiation should focus on the changing trend of the energy distribution within the entire frequency band range, instead of searching for the appearance of a certain characteristic frequency.

In this study, acoustics were selected as the basic research method, and the research was carried out starting from the acoustic characteristics of cavitation phenomena. An objective and effective identification method was explored. The proposed method was verified through model experiments to determine its correctness, thus achieving a breakthrough in cavitation monitoring methods.

2. MATERIALS AND METHODS

2.1. Analysis of the energy change law of cavitation noise

The change rule of the power spectral density of cavitation noise can be analyzed throughout the process of no cavitation, incipient cavitation, and severe cavitation.

At a high cavitation coefficient, there is no cavitation in the turbine. With the reduction of water pressure, bubbles begin to separate from the water in the turbine draft tube. These bubbles are free bubbles generated by the reduction of air solubility in the water due to pressure reduction, not cavitation. At this time, cavitation does not occur in the model turbine. The time-domain waveform of the underwater acoustic signal of the model turbine at this point is shown in Figure 2(a).

As the pressure decreases, when the pressure on the low-pressure side (usually the trailing edge of the blade) of the hydraulic turbine model runner decreases below the saturated vaporization pressure of the liquid, attached bubbles begin to appear on the blade; this is the previously defined incipient cavitation state. However, at this time, not all blades have bubbles attached, because the blade shape of the model runner is not consistent as required by theory during manufacturing. These subtle differences in processing result in the first occurrence of the attachment of bubbles on certain blades. The cavitation noise signal of the hydraulic turbine at this time is shown in Figure 2(b). Based on the time-domain waveform, sharp pulse signals already appear in the entire background sound signal. These sharp pulse signals are the sound signals radiated by the collapse of cavitation bubbles attached to the blades. At this point, the background sound of the water turbine operation is no longer sufficient to completely overshadow the sound generated by the cavitation collapse, which is the reason why human ear can be used to distinguish whether cavitation occurs or not. As the pressure continues to decrease, cavitation begins to intensify. At this point, a large number of cavitation-generated bubbles are attached to all

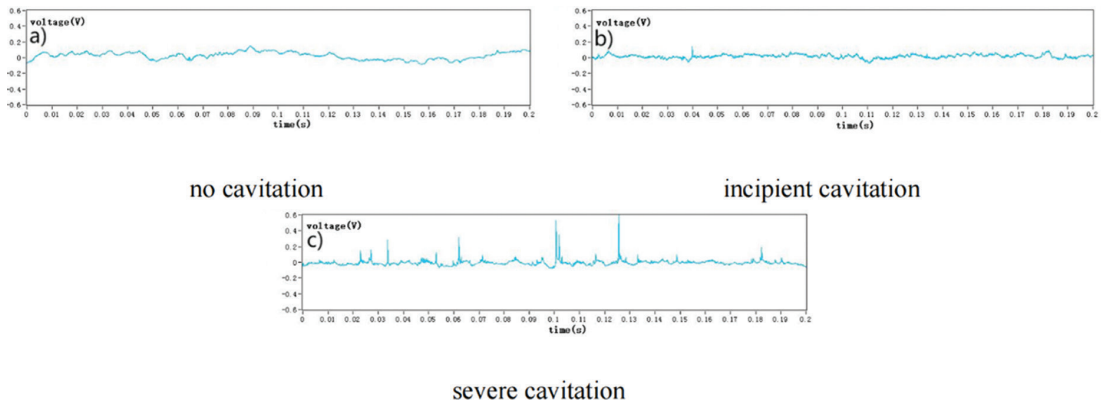

Figure 2: The waveforms of underwater acoustic signals under different cavitation coefficients.

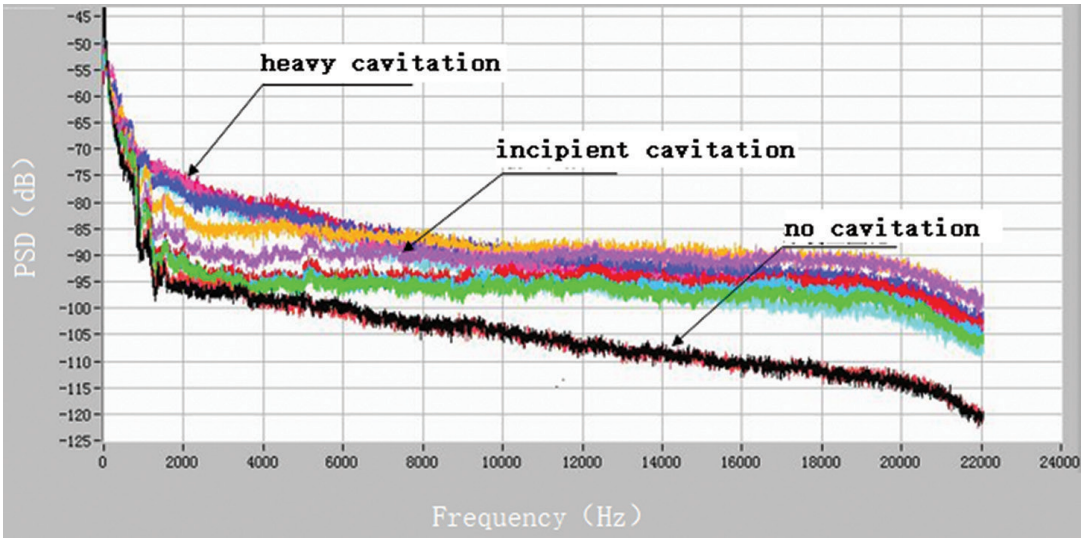

Figure 3: The variation of the power spectral density of the underwater acoustic signal during cavitation.

the model runner blades, and due to the continuous decrease in pressure, the number of free bubbles in the water continues to increase. Due to the generation and aggregation of many bubbles, a bubble group is formed. At this time, the size of the bubbles in the bubble group is much larger than that of the incipient cavitation. In addition, due to the collision and coalescence phenomena caused by the aggregation of many bubbles in the bubble group, the sound energy when the bubbles collapse is greater. From Figure 2(c), it can be seen that there are more sharp pulses as compared to those during initial cavitation, and, at this time, the peak value of the acoustic pulse signal significantly exceeds the background sound.

Figure 3 presents the change process of the power spectral density of cavitation noise signals during the entire process of cavitation occurrence and development for the model turbine. When cavitation does not occur, the low-frequency component of the noise signal is dominant and mainly composed of the water flow sound, electromagnetic noise, and other background noises of the hydraulic turbine. These background noises are characterized by a high amplitude and low frequency, and their frequencies are generally below 200 Hz; this is why the amplitude of the low-frequency component is high. As the cavitation coefficient decreases, the high-frequency energy of the signal at the beginning of cavitation significantly increases. This is because, unlike in free cavitation, the number of bubbles generated during the initial cavitation occur, and they are relatively concentrated in a certain region. The bubbles constantly repeat the process of occurrence, development, and collapse. In addition, the size of the bubbles is mainly small at this time. The energy is also more concentrated in the high-frequency region. When cavitation is very severe, the size of the bubbles increases. The frequency of the acoustic signal during bubble collapse decreases when the bubbles are larger. The power spectral density curve is significantly improved in the low-frequency region, while that of the corresponding high-frequency region begins to decrease.

In summary, the power spectral density distributions of the model hydraulic turbine before and after cavitation are not constant. The distribution changes proportionally with the onset and development of cavitation. Throughout the process, with the increase of the severity of cavitation, the energy distribution shows a trend of low frequency, followed by high frequency, which is followed again by low frequency. It is evident that the distribution of cavitation noise energy should theoretically have an extreme value as the cavitation coefficient decreases.

2.2. Extraction of time-domain features of cavitation noise signals

Figure 4 presents the time-domain waveform of a certain model hydraulic turbine at the cavitation coefficients of 0.16, 0.14, 0.12, 0.1, 0.09, 0.08, 0.07, and 0.06, respectively.

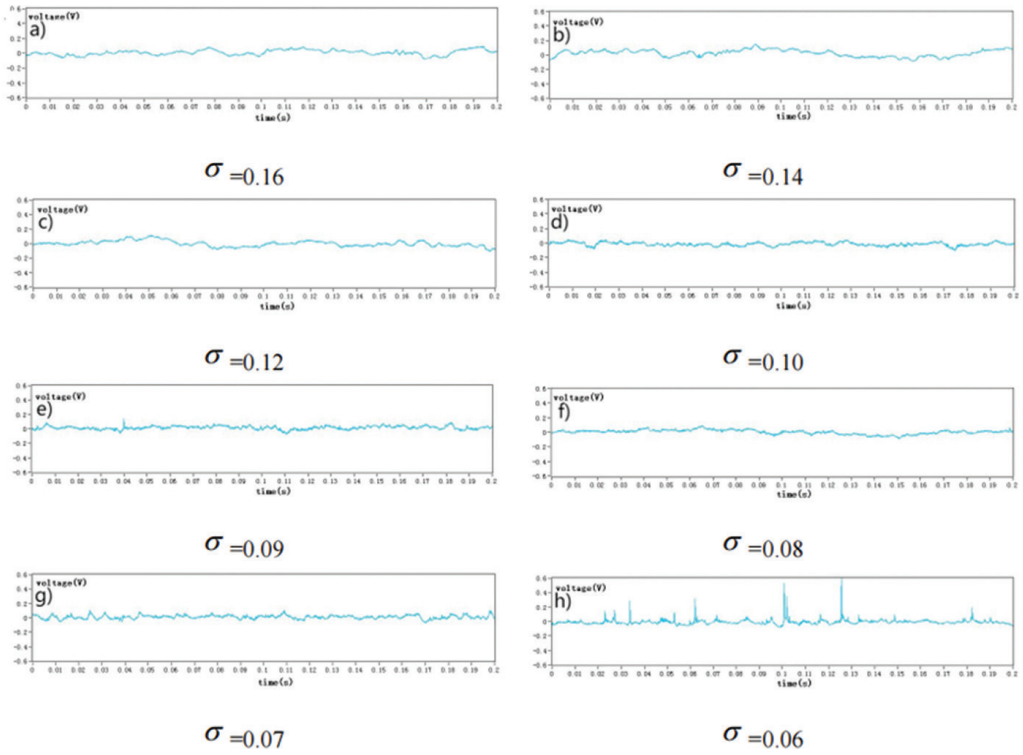

Figure 4: The time-domain waveforms of cavitation noise under different cavitation coefficients.

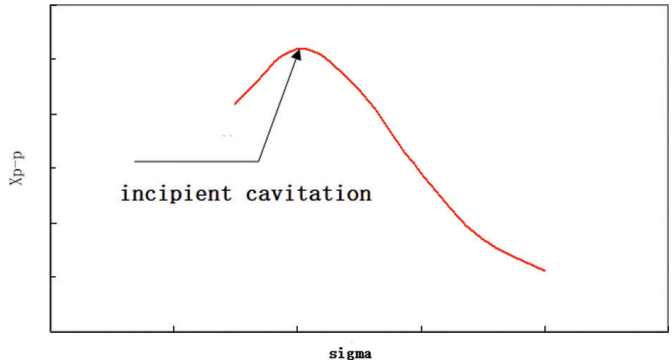

Figure 5: The variation of the peak-to-peak value of cavitation noise with the cavitation coefficient.

The magnitude of energy is characterized by peak-to-peak values. According to the previous analysis, before the occurrence of initial cavitation, the peak-to-peak values increase with the decrease of the cavitation coefficient, and a local maximum value appears at the initial cavitation coefficient. As the cavitation coefficient decreases, due to the occurrence of a strong coalescence phenomenon, the sound energy shifts toward the low-frequency direction, resulting in a decrease in energy. This occurs until the cavitation phenomenon is very severe, after which the peak-to-peak value increases sharply. Figure 5 presents the theoretical trend of the peak-to-peak value of the cavitation noise signal with the cavitation coefficient (The Xp-p means peak-to-peak value of the final noise signal. Sigma means cavitation coefficient).

In order to process the collected noise signals during subsequent experiments, mathematical language is used to represent the noise signals. Assuming that the time-domain signal of cavitation noise is $x(t)$, after sampling and discretization, it is $x(n)$. To eliminate the interference of signals with a large deviation, the discrete time-domain signal of cavitation noise is extracted within a certain confidence interval, as follows.

First, the mean of each set of sampled signals is calculated; then,

$$\overline{x} = \frac{1}{n}\sum_{i=1}^{n} x_i \tag{1}$$

According to the Bessel Formula, the standard deviation of the signal is calculated using the mean value of the sound signal; then,

$$s(x) = \sqrt{\frac{1}{n}\sum_{i=1}^{n} V_i} = \sqrt{\frac{1}{n}\sum_{i=1}^{n}(x_i - \overline{x})} \tag{2}$$

Taking a confidence interval ($\overline{x} - 2.576s$, $\overline{x} + 2.567s$) with a confidence probability of 99% as the standard for constructing the final signal sample space, the final sample space $x_i'(i = 1,2,..., n)$ is formed. The new signal value satisfies the condition that all the values fall within a confidence interval ($\overline{x} - 2.576s$, $\overline{x} + 2.567s$) with a confidence probability of 99%. All the values outside this range are replaced by the mean of the signal $\overline{x}$, thereby eliminating significant interference from the original signal.

The peak-to-peak value of the final noise signal that eliminates interference with a large deviation is

$$x_{p-p} = \max\left\{x_i'\right\} - \min\left\{x_i'\right\} \tag{3}$$

2.3. Extraction of frequency-domain features of the cavitation noise signal

To obtain the energy distribution relationship of the cavitation noise signal in the frequency domain, the power spectral density of the collected cavitation noise signal in the frequency domain is analyzed, and the power spectral density curve is shown in Figure 6.

In the frequency domain, due to the distribution proportions of high- and low-frequency energy, the frequency of the boundary point changes with the cavitation coefficient. This frequency is defined as the inflection point frequency, represented by f_{BP}, as shown in Figure 7.

To accurately calculate the proportions of high- and low-frequency energy and quantitatively represent the distribution trend of energy, it is necessary to accurately define the inflection point frequency f_{BP}. According to the distribution trend of noise energy in the spectrum, the power spectral density curve is fitted with a piecewise function to accurately determine the inflection point frequency value, as shown in Figure 8.

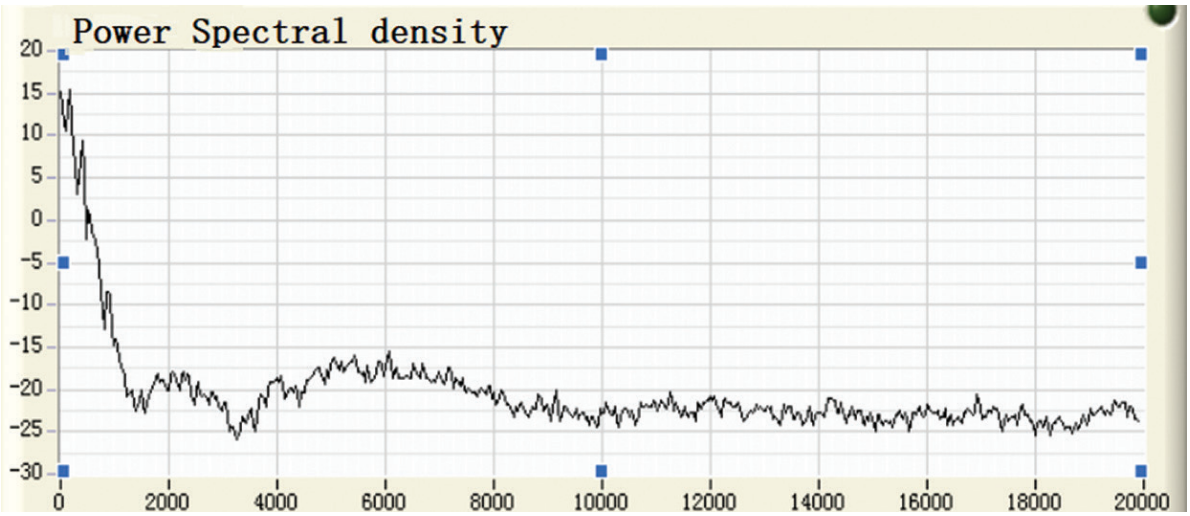

Figure 6: The power spectral density curve.

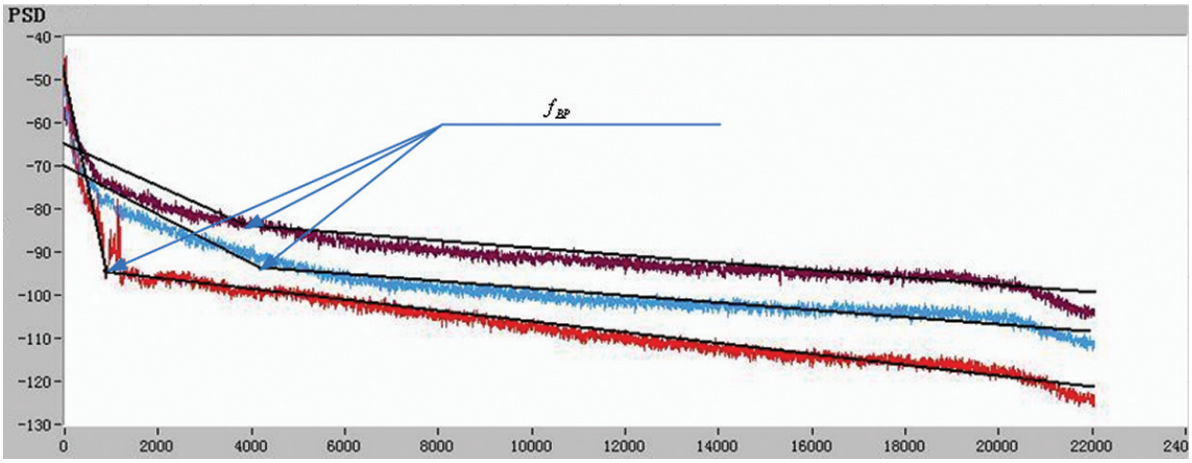

Figure 7: The definition of the inflection point frequency.

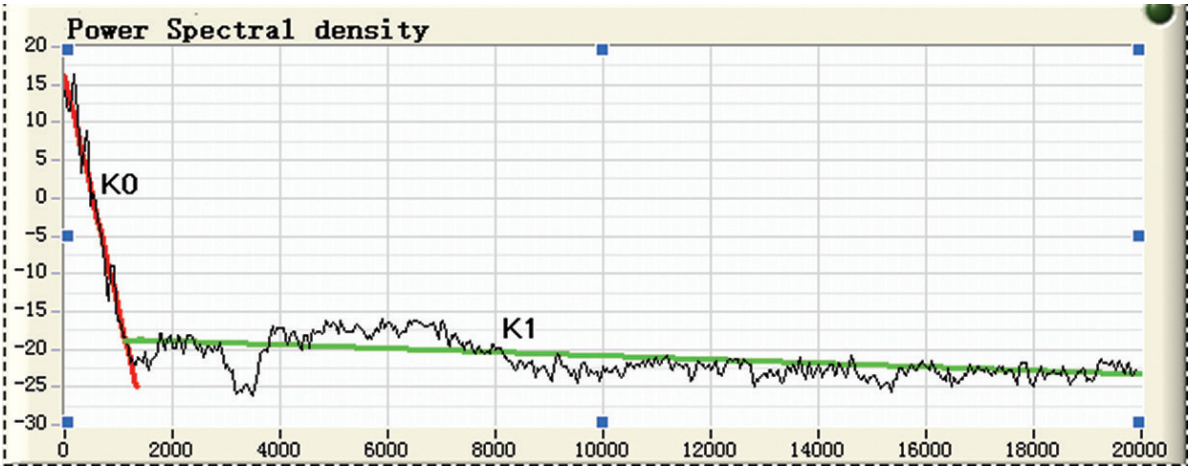

Figure 8: The fitting of the power spectrum curve with a piecewise function.

For each unit monitoring data (x_i, y_i), according to error analysis theory, the residual is $V_i x(n)$. If $V_i = y_i - \bar{y}_i$ and x_m is the inflection point frequency, then

$$V_i = \begin{cases} y_i - k_0 x_i - b_0, x_i \le x_m \\ y_i - k_1 x_i - b_1, x_i \le x_m \end{cases} \tag{4}$$

If when $x_i \le x_m$, the frequency number is n_1;

If when $x_i > x_m$, the frequency number is n_2;

Then, $n_1 + n_2 = N$, where N is the total number of all frequency values contained in the power spectrum after Fourier transform. Then,

$$Q_i = \sum_{i=1}^{N} V_i^2 = \sum_{i=1}^{n_1} V_i^2 = \sum_{i=1}^{n_2} V_i^2 \tag{5}$$

If $\frac{\partial Q_i}{\partial k_0} = 0$, $\frac{\partial Q_i}{\partial k_1} = 0$, $\frac{\partial Q_i}{\partial b_0} = 0$, and $\frac{\partial Q_i}{\partial b_1} = 0$, then

$$\begin{cases} a_1 k_0 + a_2 b_0 = c_1 \\ a_2 k_0 + a_3 b_0 = c_2 \end{cases} \tag{6}$$

$$\begin{cases} a_1' k_1 + a_2' b_1 = c_1' \\ a_2' k_1 + a_3' b_1 = c_2' \end{cases} \tag{7}$$

Then, the following is true.

$$\begin{aligned} a_1' &= \sum_{i=1}^{n_2} x_i^2 \quad a_1 = \sum_{i=1}^{n_1} x_i^2 \\ a_2' &= \sum_{i=1}^{n_2} x_i \quad a_2 = \sum_{i=1}^{n_1} x_i \\ a_3' &= \sum_{i=1}^{n_2} \quad a_3 = \sum_{i=1}^{n_1} \\ c_1' &= \sum_{i=1}^{n_2} y_i x_i \quad c_1 = \sum_{i=1}^{n_1} y_i x_i \\ c_2' &= \sum_{i=1}^{n_2} y_i \quad c_2 = \sum_{i=1}^{n_1} y_i \end{aligned} \tag{8}$$

To find the best-fitting curve, x_m is added in the form of $x_m = x_0 + ih$, where i = 1,2,3 ... N–1, and h is the frequency resolution. When the sum of squares of the residuals Q_i is the smallest, the frequency value corresponding to the minimum value x_m is the inflection point frequency f_{BP}. This means that under a certain operating condition, as the cavitation coefficient decreases, the cavitation coefficient corresponding to the maximum value of f_{BP} is the initial cavitation coefficient of the turbine under that operating condition.

Taking the inflection point frequency f_{BP} as the dividing point, the power spectral density curve of the cavitation noise signal is clearly divided into the high-frequency and low-frequency parts. The distribution trends of the signal energy of the two parts can respectively be expressed by the slopes k_0 and k_1 of the first-order piecewise function. Then, the following can be obtained.

$$k_0 = \frac{\sum_{i=1}^{n_1} y_i \times \sum_{i=1}^{n_1} x_i - \sum_{i=1}^{n_1} y_i x_i \times \sum_{i=1}^{n_1}}{\left(\sum_{i=1}^{n_1} x_i\right)^2 - \sum_{i=1}^{n_1} x_i^2 \times \sum_{i=1}^{n_1}} \tag{9}$$

$$k_1 = \frac{\sum_{i=1}^{n_2} y_i \times \sum_{i=1}^{n_2} x_i - \sum_{i=1}^{n_2} y_i x_i \times \sum_{i=1}^{n_2}}{\left(\sum_{i=1}^{n_2} x_i\right)^2 - \sum_{i=1}^{n_2} x_i^2 \times \sum_{i=1}^{n_2}} \tag{10}$$

$$k_0/k_1 = \left[\frac{\sum_{i=1}^{n_1} y_i \times \sum_{i=1}^{n_1} x_i - \sum_{i=1}^{n_1} y_i x_i \times \sum_{i=1}^{n_1}}{\left(\sum_{i=1}^{n_1} x_i\right)^2 - \sum_{i=1}^{n_1} x_i^2 \times \sum_{i=1}^{n_1}}\right] \Bigg/ \left[\frac{\sum_{i=1}^{n_2} y_i \times \sum_{i=1}^{n_2} x_i - \sum_{i=1}^{n_2} y_i x_i \times \sum_{i=1}^{n_2}}{\left(\sum_{i=1}^{n_2} x_i\right)^2 - \sum_{i=1}^{n_2} x_i^2 \times \sum_{i=1}^{n_2}}\right] \tag{11}$$

At a certain operating point, as the cavitation coefficient decreases, the cavitation coefficient corresponding to the minimum value of k_0/k_1 is the initial cavitation coefficient.

$$E_0 = \sum_{i=0}^{n_1-1} y_i h \tag{12}$$

$$E_1 = \sum_{i=n_1}^{N-1} y_i h \tag{13}$$

$$E_0/E_1 = \left(\sum_{i=0}^{n_1-1} y_i \cdot h\right) \Bigg/ \left(\sum_{i=n_1}^{N-1} y_i \cdot h\right) \tag{14}$$

Based on the preceding analysis, the distribution trend and proportions of high- and low-frequency energy should theoretically have extreme values, as shown in Figure 9.

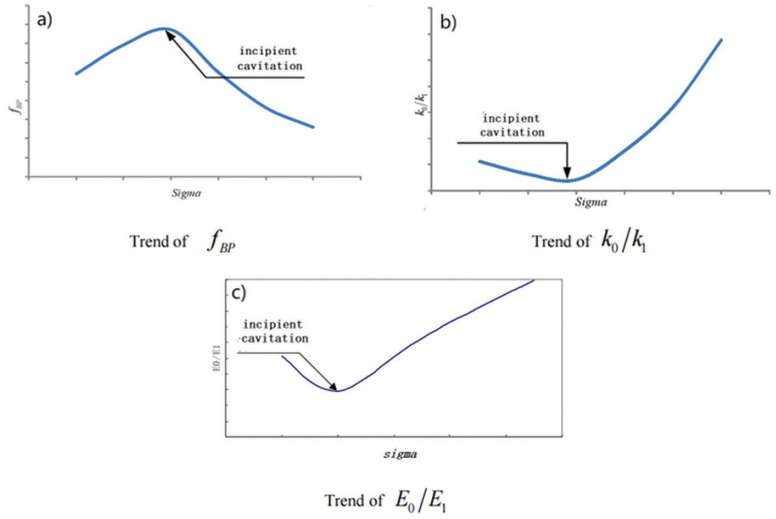

Figure 9: The curves of the changes of high- and low-frequency energy parameters with the cavitation coefficient.

3. RESULT AND DISCUSSION

3.1. Model test bench and model cavitation test

To verify the accuracy and effectiveness of this initial cavitation determination method, a high-parameter and high-precision hydraulic machinery testing device was used for model cavitation testing. The model device parameters are shown in Table 1.

In the model cavitation test, an imaging observation system was used to observe the cavitation state at the runner blade outlet. The schematic diagram of the test equipment is shown in Figure 10. A hydrophone was installed at the transparent cone of the model device as close as possible to the runner outlet, and the installation position is shown in Figure 11. The noise signal collected by the hydrophone is processed by a charge amplifier and transmitted to the sound card on the PC to achieve digitization. The digitized data is analyzed and mathematically calculated by the testing system software, which is mainly written in LabVIEW. The exhaust valve was closed during model testing. The vacuum pump and valve were operated to extract air from the system to reduce the draft tube pressure, thereby reducing the cavitation coefficient. The test personnel observed the occurrence of cavitation on the blades by adjusting the stroboscopic device. When cavitation was about to occur, the turbine reached the initial cavitation state via the combination of the exhaust and extraction valves. The experimenter recorded the cavitation coefficient at this point, which was the initial cavitation coefficient. Another group of experimenters used the acoustic method developed in this study to collect cavitation noise data, and conducted the real-time analysis of the data to obtain the curves of cavitation noise time and frequency domain criteria changing with cavitation coefficient. After the initial cavitation occurred, the draft tube pressure was continually reduced until the efficiency decreased by 1%, and the experiment was ended. After the experiment, the observed results were compared with the data analysis results collected by the acoustic method to verify the effectiveness of the acoustic method.

Table 1: The model device parameters.

PARAMETERS	DIMENSION	UNIT
Max hydraulic head	150	m H_2O
Max flow rate	2.0	m^3/s
Diameter of runner	200–500	mm
Power	500	kW
Speed	0~2500	r/min
Efficiency error	≤±0.20	%

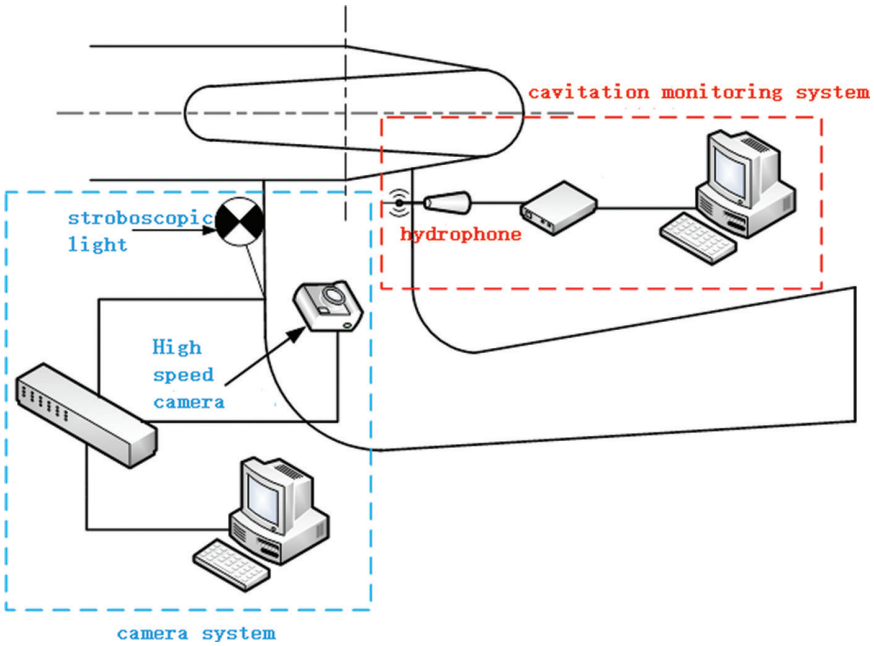

Figure 10: The schematic diagram of the experimental model equipment.

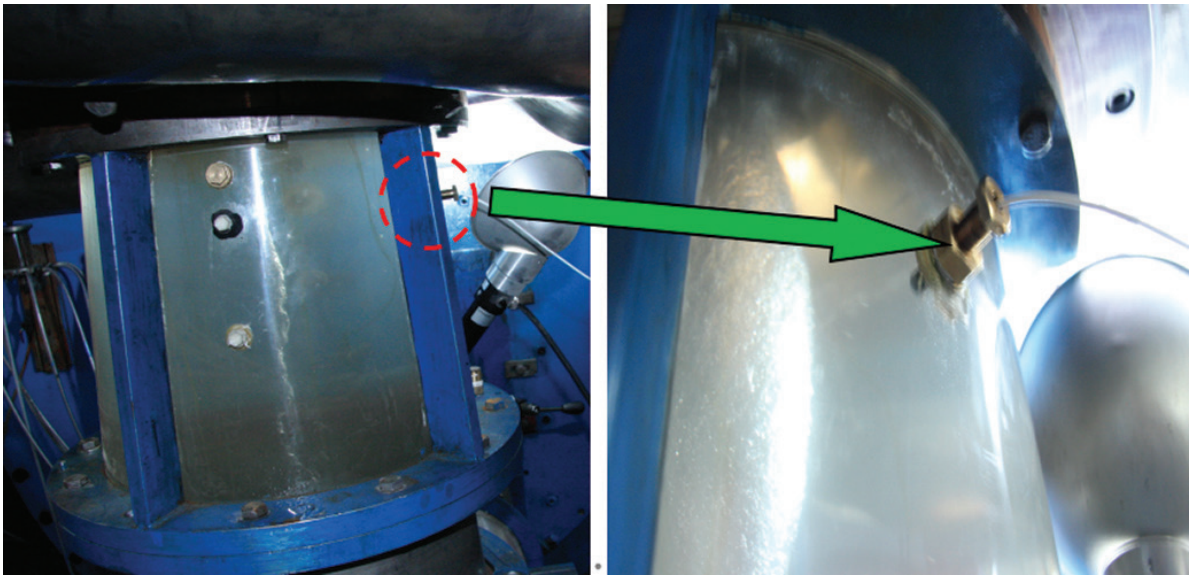

Figure 11: The installation position of the hydrophone.

3.2. Experimental verification of cavitation under pump operating conditions of pump turbine

The accuracy of the acoustic method for determining incipient cavitation of pump turbines during the application of the pump operating conditions was verified by conducting experimental research on incipient cavitation on hydraulic machinery testing devices. The basic parameters of the pump turbine are shown in Table 2.

Two typical operating points were selected for comparative verification in the model experiment, the parameters of which are reported in Table 3. OP1 was selected in the low-flow area of the pump condition. The cavitation inception of the model runner in OP1 occurred at the inlet edge of the suction surface of the runner blade. OP2 was selected in the high-flow area of the pump condition. The incipient cavitation in OP2 occurred on the pressure surface of the inlet side of the runner blade, and only when the cavitation was severe did the cavitation cloud transition to the suction surface of the inlet side of the runner blade.

Figure 12 shows the incipient cavitation observed by the high-speed camera system at OP1. The attachment of bubbles to the roots of the suction surface blades of #8 and #3, as marked with red dashed lines, indicates the occurrence of incipient cavitation. These results were compared with the results of acoustic analysis, which are presented in Figure 13. The trend of the curve shows that the time- and frequency-domain mathematical models respectively reached maximum and minimum values as the cavitation coefficient decreased. The cavitation coefficients corresponding to the extreme values of the time- and frequency-domain mathematical model values were the same and completely consistent with the initial cavitation results observed using the high-speed camera system. The same conclusion was obtained from the test results at the OP2 operating point.

Table 2: The parameters of the model pump turbine.

DIAMETER OF RUNNER D1	NUMBER OF BLADES	NUMBER OF GUIDE VANES	RELATIVE HEIGHT OF GUIDE VANES B0/D1
0.25 m	9	20	0.1253

Table 3: The parameters of the test points.

OPERATING POINTS	HEAD H	FLOW RATE Q
OP1	35.72 m	219.3 l/s
OP2	31.05 m	273.2 l/s

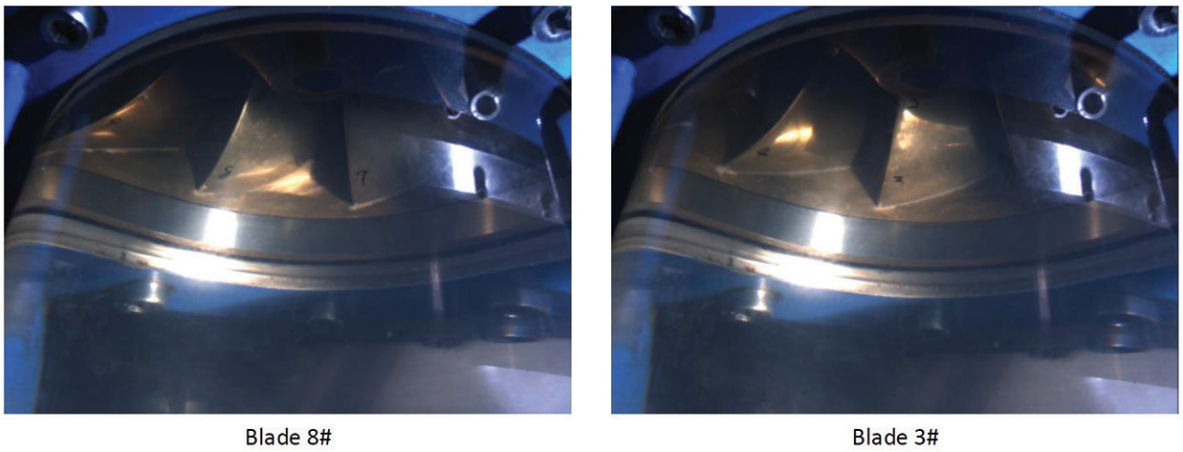

Figure 12: The observation of incipient cavitation at OP1 at the cavitation coefficient (σ) of 0.12.

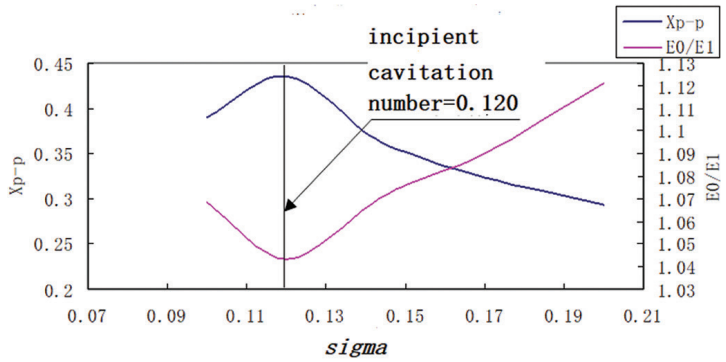

Figure 13: The change of the time- and frequency-domain mathematical models with the cavitation coefficient at OP1.

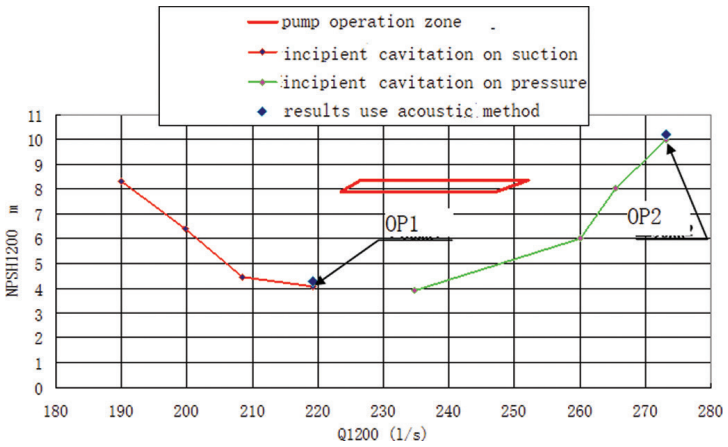

Figure 14: The comparison between traditional observation methods and acoustic cavitation inception points.

By comparing the experimental results of the two operating points, as shown in Figure 14, it can be seen that the results of using the proposed acoustic method to determine the initial cavitation value of the model pump turbine blade under the pump operating conditions were very consistent with the experimental results obtained using traditional observation methods.

3.3. Experimental verification of initial cavitation in the model hydraulic turbine

Second, the accuracy of the application of the proposed acoustic method in determining incipient cavitation on a Francis turbine was verified. The incipient cavitation was experimentally investigated using hydraulic machinery testing devices. The basic parameters of the turbine are reported in Table 4.

Two operating points were selected, the parameters of which are listed in Table 5. Figure 15 presents the observation results of the incipient cavitation test of the Francis turbine at OP3. Small cavitation groups obviously appeared at the blade root of the marked area in the figure, indicating the occurrence of the incipient cavitation of the model turbine. The comparison between the observation results and the results of the acoustic method is provided in Figure 16. The incipient cavitation coefficients determined by both methods were 0.089. In the test process of the acoustic method, as the cavitation coefficient decreased, the inflection point frequency f_{BP} first presented a monotonically increasing trend. When the cavitation coefficient reached 0.089, a maximum value appeared, and as the cavitation coefficient further decreased, f_{BP} exhibited a monotonically decreasing trend. The frequency-domain mathematical model k_0/k_1 first exhibited a monotonically decreasing trend, with

Table 4: The parameters of the model turbine.

DIAMETER OF RUNNER D1	NUMBER OF BLADES	NUMBER OF GUIDE VANES	RELATIVE HEIGHT OF GUIDE VANES B0/D1
0.42 m	16	24	0.1825

Table 5: The parameters of the test points.

OPERATING POINTS	HEAD H	FLOW RATE Q
OP3	25 m	579.1 l/s
OP4	25 m	575.6 l/s

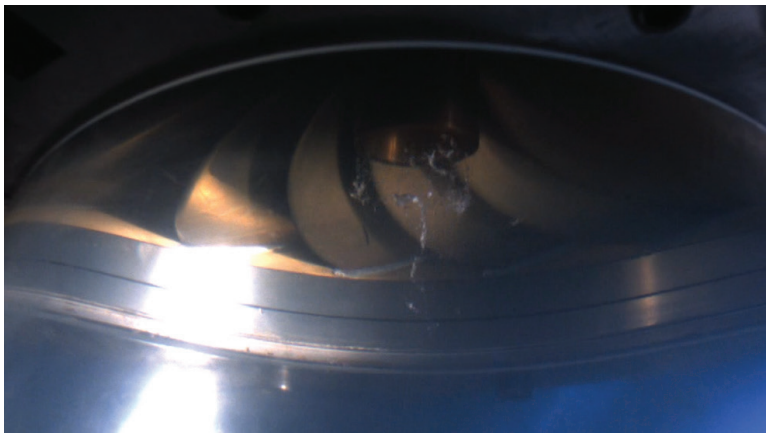

Figure 15: The observational images of incipient cavitation at OP3 when $\sigma = 0.089$.

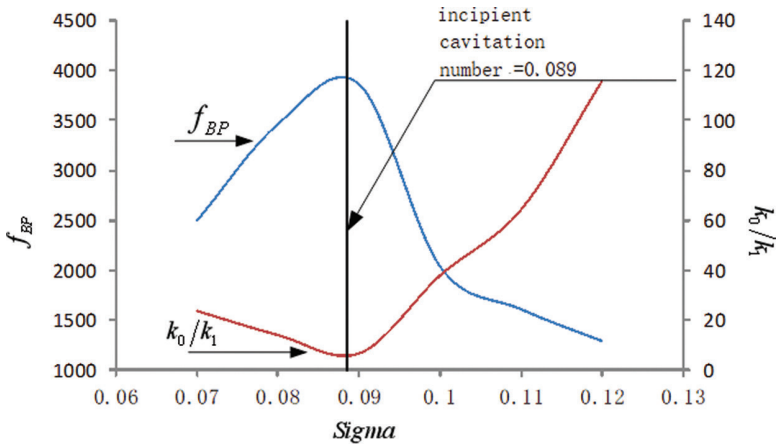

Figure 16: The variation of the inflection point frequency and energy variation trend ratio with the cavitation coefficient.

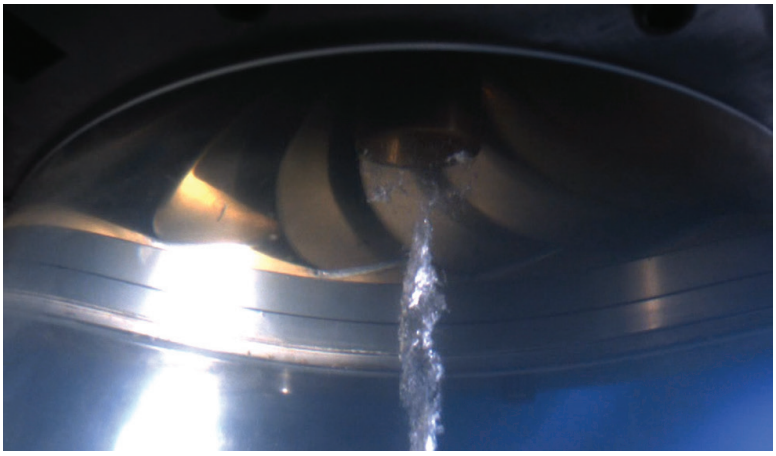

Figure 17: The observational images of incipient cavitation at OP4 when $\sigma = 0.081$.

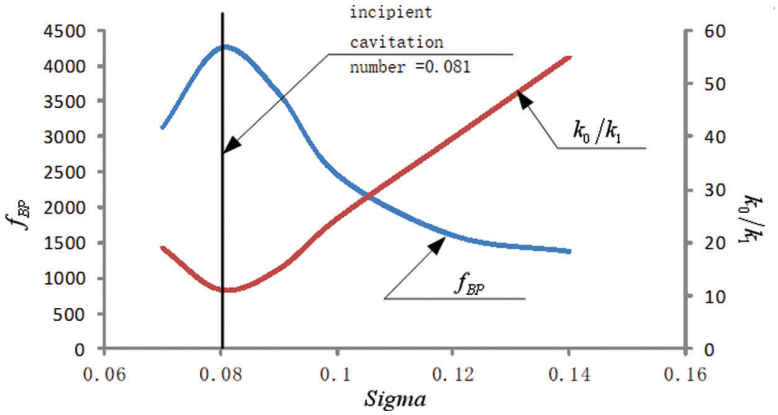

Figure 18: The variation of the inflection point frequency and energy variation trend ratio with the cavitation coefficient.

a minimum value appearing when the cavitation coefficient dropped to 0.089. As the cavitation coefficient decreased again, k_0/k_1 presented a monotonically increasing trend.

Figure 17 displays the observation results of the incipient cavitation of the Francis turbine model at OP4. Small cavitation groups also appeared at the blade root after the reverse columnar vortex belt, indicating the incipient cavitation state of the turbine. The results of the acoustic method are shown in Figure 18. The incipient cavitation coefficients determined by both methods were 0.081. The value of f_{BP} first presented a monotonically increasing upward trend. When the cavitation coefficient reached 0.081, a maximum value appeared, and as the cavitation further decreased, f_{BP} showed a monotonically decreasing trend. The frequency-domain mathematical model k_0/k_1 first presented a monotonically decreasing trend, with a minimum value appearing when the cavitation coefficient dropped to 0.089. As the cavitation coefficient decreased again, k_0/k_1 exhibited a monotonically increasing trend.

4. CONCLUSIONS

This article summarized the energy distribution of initial cavitation noise and its variation with the cavitation coefficient via the theoretical research and analysis of radiation sound energy during cavitation occurrence, in combination with model experiments. The following conclusions were drawn.

1. The peak-to-peak value representing the time-domain energy increases with the decrease of the cavitation coefficient, and an extreme value appears near the initial cavitation. However, as cavitation further intensifies, the peak-to-peak value sharply increases.
2. By fitting the spectral density curve of the internal power rate in the frequency domain with the least-squares method, the frequency of the energy boundary point in the high- and low-frequency regions is defined as the inflection point frequency. The inflection point frequency has an extreme value near the incipient cavitation, indicating that the distributions of high- and low-frequency energy will change significantly near the incipient cavitation.

3. The slopes of the fitting curves and their ratios in the high- and low-frequency regions decrease with the increase of the cavitation coefficient, and a minimum value appears near the initial cavitation.
4. The acoustic method developed in this study is accurate and effective for the quick and non-contact judgment of cavitation inception.

5. ACKNOWLEDGMENTS

This work was supported by the LiaoNing Revitalization Talents Program (Grant No. XLYC2007083), the Liaoning BaiQianWan Talents Program (Grant No. LNBQW2020Q0141), the Talent Scientific Research Fund of LSHU (Grant No. 2020XJJL-010), and the Open Research Fund of State Key Laboratory of Hydro-Power Equipment (Grant No. SKLHE-ORF-202108).

6. BIBLIOGRAPHY

[1] PLESSET, M.S., "The dynamics of cavitation bubbles", *Journal of Applied Mechanics*, v. 16, n. 3, pp. 277–282, 1949. doi: http://dx.doi.org/10.1115/1.4009975.

[2] ZHAO, G., CAO, L., CHE, B., *et al*., "Towards the control of blade cavitation in a waterjet pump with inlet guide vanes: Passive control by obstacles", *Ocean Engineering*, v. 231, n. 6, pp. 108820, 2021. doi: http://dx.doi.org/10.1016/j.oceaneng.2021.108820.

[3] YAN, Z., LIU, J., CHEN, B., *et al*., "Fluid cavitation detection method with phase demodulation of ultrasonic signal", *Applied Acoustics*, v. 87, pp. 198–204, 2015. doi: http://dx.doi.org/10.1016/j.apacoust.2014.07.007.

[4] TIWARI, R., BORDOLOI, D.J., DEWANGAN, A., "Blockage and cavitation detection in centrifugal pumps from dynamic pressure signal using deep learning algorithm", *Measurement*, v. 173, n. 1, pp. 108676, 2021. doi: http://dx.doi.org/10.1016/j.measurement.2020.108676.

[5] BAJIC, B., "Multi-dimensional diagnostics of turbine cavitation", *Journal of Fluids Engineering*, v. 124, n. 4, pp. 943–950, 2002. doi: http://dx.doi.org/10.1115/1.1511162.

[6] Power Online SM, *Model 7915 Cavitation Monitoring System*, www.poweronline.com/product.mvc/Model-7915-Cavitation-Monitoring-System-0001, accessed in July, 2023.

[7] ESCALER, X., EGUSQUIZA, E., FARHAT, M., *et al*., "Cavitation erosion prediction in hydro turbines from onboard vibrations", In: *Proceedings of IAHR Symposium on Hydraulic Machinery & Systems*, 2004.

[8] PENDAR, M.R., PASCOA, J.C., "Numerical investigation of plasma actuator effects on flow control over a three-dimensional airfoil with a sinusoidal leading edge", *Journal of Fluids Engineering Transactions of the ASME*, v. 144, n. 8, pp. 081208, 2022. doi: http://dx.doi.org/10.1115/1.4053847.

[9] KOLAHAN, A., ROOHI, E., PENDAR, M.R., "Wavelet analysis and frequency spectrum of cloud cavitation around a sphere", *Ocean Engineering*, v. 182, n. 15, pp. 235–247, 2019. doi: http://dx.doi.org/10.1016/j.oceaneng.2019.04.070.

[10] ČUDINA, M., "Detection of cavitation phenomenon in a centrifugal pump using audible sound", *Mechanical Systems and Signal Processing*, v. 17, n. 6, pp. 1335–1347, 2003. doi: http://dx.doi.org/10.1006/mssp.2002.1514.

[11] HU, F., CHEN, T., WU, D., *et al*., "Experiment study of cavitation induced vibration and noise of guide vane mixed flow pump", *Paiguan Jixie Gongcheng Xuebao*, v. 31, n. 12, pp. 1021–1024, 2013.

[12] LIU, Z., CHEN, Y., XIONG, Z., *et al*., "Study on time and frequency domain characteristics of propeller cavitation noise", In: *Symposium on Underwater Noise from Ships*, 2013.

[13] RAMADEVI, R., "Classification of vibration signal to detect pump cavitation using discrete wavelet transform", *International Journal of Computers and Applications*, v. 93, n. 10, pp. 36–39, 2014. doi: http://dx.doi.org/10.5120/16254-5864.

[14] HE, Y., LIU, Y., "Experimental research into time-frequency characteristics of cavitation noise using wavelet scalogram", *Applied Acoustics*, v. 72, n. 10, pp. 721–731, 2011. doi: http://dx.doi.org/10.1016/j.apacoust.2011.03.008.